

Geometrical constraints on plasma couplers for Raman compression

Z. Toroker,¹ V. M. Malkin,² A. A. Balakin,³ G. M. Fraiman,³ and N. J. Fisch^{1,2}

¹Princeton Plasma Physics Laboratory, Princeton, New Jersey 08543, USA

²Department of Astrophysical Sciences, Princeton University, Princeton, New Jersey 08544, USA

³Institute of Applied Physics RAS, Nizhny Novgorod 603950, Russia

(Received 16 May 2012; accepted 31 July 2012; published online 23 August 2012)

Backward Raman compression in plasma is based on a 3-wave resonant interaction, which includes two counter-propagating laser pulses (pump and seed pulses) and an electron plasma wave (Langmuir wave). The resonant interaction can be ensured in nearly homogeneous plasmas. However, for high-power, large-aperture experiments, the homogeneous region becomes pancake-shaped and would likely be surrounded by thicker regions of inhomogeneous plasma. When these inhomogeneous plasma regions are extensive, significant inverse bremsstrahlung and seed dispersion may impede the compression effect. These deleterious effects may, however, be mitigated by chirping the seed and pump pulses. © 2012 American Institute of Physics. [<http://dx.doi.org/10.1063/1.4745868>]

I. INTRODUCTION

Resonant backward Raman amplification (BRA)¹ in plasma may enable the next generation high intensity laser pulses. In this approach, the dielectric grating limitation of the chirped pulse amplification (CPA)² is overcome through the use of plasma medium.

The BRA scheme consists of two counter-propagating laser pulses, a long pump pulse and a short seed pulse, which propagate in a plasma medium. When the pulses begin to overlap, the long pump pulse transfers part of its energy to the short seed pulse via the mediation of the Langmuir wave. The mechanism comprises both amplification and compression of the short counter-propagating seed, which produces an output pulse much shorter than the pump pulse but with almost all the energy of the pump pulse. Because the energy in the long pump pulse is transformed to energy in the much shorter output seed pulse, we call this mechanism *Raman compression*. This mechanism continues to attract considerable attention, including theoretical, experimental, and computational, as well as extrapolation to regimes not originally contemplated.^{3–38} Moreover, by including chirped pulse amplification, together with Raman compression, the advantages of both schemes can be realized together for the highest intensity applications.¹⁴

The most effective transfer of energy from pump to seed pulse occurs when the Raman resonance condition is satisfied. However, in practical realizations of the plasma, there will be a homogeneous middle section flanked by inhomogeneous plasma end sections. For given pump and seed frequencies, the Raman resonance condition is then generally satisfied only in the homogeneous plasma section. The inhomogeneous sections do not contribute much to the compression effect, but could impede it.

While the neglect of substantive effects in the end regions may be appropriate for describing the first generation of Raman compression experiments,^{1,3–38} this approximation may not be appropriate for the next generation of intensities. This is because the first generation of experiments is in the

limit of what we can call *high aspect ratio plasma*, where the plasma cross sectional dimension is small compared to the length of the homogeneous region. Since in such structures most of the plasma is homogeneous, it is generally justified to assume theoretically that the interaction is dominated by the physics of the central homogeneous region.

However, to achieve the next generation of intensities, significant transverse focusing will be required in addition to the longitudinal compression, so a large laser spot size will be required to process more power for the Raman compression. The optimal length of the plasma homogeneous section¹ will then be shorter than the transverse size, resulting in what might be called a *low aspect ratio plasma*. In the *low aspect ratio* limit, the plasma would be shaped like a pancake. However, pancake-shaped homogeneous plasmas are not easily produced. The falloff in density in the axial direction could easily be on the order of or even greater than the width of the homogeneous central section. The concern is that deleterious effects in these larger non-resonant regions may reduce the Raman compression.

To determine quantitatively how the inhomogeneous plasma regions can affect the Raman compression, we consider here a plasma slab that comprises a homogeneous middle section and two symmetrically placed inhomogeneous end sections, such that the electron density in each end section decreases to zero. We call the total length from each edge of the homogeneous section to the point where the plasma density decreases by half the *plasma coupler tail length*.

The example of particular interest for us is when the homogeneous section is of a relatively high density, which produces the shortest output pulses and hence the greatest compression effect, but which also is most susceptible to the effects of seed dispersion and inverse bremsstrahlung. We show that, for plasma coupler tail length longer than the length of the homogeneous section, as we expect to find in the next generation of Raman compression experiments, the Raman compression tends to be significantly reduced due to the seed dispersion and the inverse bremsstrahlung. However, as we also show, chirping of both the seed and the

pump pulses enables efficient resonant BRA in most of the inhomogeneous plasma. Thus, the amplified seed passes through shorter a non-resonant plasma region, so it will be less affected by deleterious effects.

This paper is organized as follows: Sec. II gives the coupled 3-wave equations that describe the Raman amplification. It also gives the electron heat equation, derived from a one dimensional fluid model. In Sec. III, we show numerically that the Raman compression efficiency is affected by both the plasma coupler tail length and the initial pump intensity. In Sec. IV, we show that proper chirping of both the pump and seed can partially overcome the deleterious seed dispersion and the inverse bremsstrahlung effects. Conclusions are given in Sec. V.

II. MODEL DESCRIPTION

The one dimensional normalized backward Raman compression model can be described by the coupled 3-wave equations^{19,24,26}

$$\begin{aligned} a_t + a_z c_a / c &= q_n^{1/4} b f + i \sigma_a a - \nu_a a, \\ b_t - b_z c_b / c &= -q_n^{1/4} a f^* + i \sigma_b b - i \kappa b_t + i R |b|^2 b - \nu_b b, \\ f_t &= -q_n^{1/4} a b^* + i \sigma_f f - \nu_f f, \end{aligned} \quad (1)$$

and the electron heat equation³⁹

$$\frac{\partial 3}{\partial t 2} q_T = \nu_{ei} (T_a + T_b + T_f) / T_m + 2 \nu_{Lnd} T_f / T_m, \quad (2)$$

where a and b are the normalized amplitudes of the circularly polarized vector potentials of the pump and the seed pulses such that the amplitudes of the vector potentials are measured in units of $a_0 m_e c^2 / e$ and $\sqrt{\omega_a / \omega_b} a_0 m_e c^2 / e$, respectively. Also, f is the normalized amplitude of the electrostatic electric field of the Langmuir wave such that the amplitude of the electric field is measured in units of $\sqrt{2 \omega_a \omega_e} a_0 m_e c / e$. Here, the frequency of the pump laser and the seed laser are ω_a and ω_b , respectively. The electron plasma frequency is $\omega_e = \sqrt{4 \pi n_h e^2 / m_e}$, where m_e is the electron mass, e is the electron charge, n_h is the electron density in the homogeneous section, and c is the speed of light in vacuum. The initial normalized pump amplitude is $a_0 = \lambda_a \sqrt{I_{a0} / \pi c} / m_e c^2 / e \approx 6 \cdot 10^{-6} \lambda_a \sqrt{I_{a0}}$, where λ_a is the pump wavelength in vacuum measured in cm and I_{a0} is the initial pump intensity measured in W/cm².

The group velocity of the pump is $c_a = c \sqrt{1 - \omega_e^2 / \omega_a^2}$ and the group velocity of the seed is $c_b = c \sqrt{1 - \omega_e^2 / \omega_b^2}$. The time t is measured in units of $1 / V_3 a_0$ and the distance z in units of $c / V_3 a_0$, where $V_3 = (k_f c / 2) \sqrt{\omega_e / 2 \omega_b}$ is the 3-wave coupling constant.⁴⁰ The resonant Langmuir wave number, k_f , in the homogeneous section is $k_f = k_a + k_b$, where $k_a c = \sqrt{\omega_a^2 - \omega_e^2}$ and $k_b c = \sqrt{\omega_b^2 - \omega_e^2}$. The frequency resonance condition in the homogeneous section is $\omega_a = \omega_b + \omega_f$, where $\omega_f = \omega_e \sqrt{1 + 3 q_T}$ is the resonant

Langmuir frequency and $q_T = k_f^2 T_e / \omega_e^2 m_e = T_e / T_m$ is the electron temperature measured in T_m . We assume that the plasma is cold enough such that $\omega_f \approx \omega_e$.

The plasma inhomogeneity induces detuning from the homogeneous resonance condition. The detuning coefficients of the pump, seed, and Langmuir wave pulses are $\sigma_a = \omega_e^2 (q_n - 1) / 2 V_3 \omega_a$, $\sigma_b = \omega_e^2 (q_n - 1) / 2 V_3 \omega_b$, and $\sigma_f = \omega_e^2 (q_n - 1) / 2 V_3 \omega_f$, where $q_n = n_e(z) / n_h$ is the normalized electron density. The expressions given here for $\sigma_{a,b,f}$ are derived from the vector potential wave equation, using the slowly varying envelope approximation for the pump, seed, and Langmuir waves. These expressions are valid for arbitrarily large plasma inhomogeneities, not only in the limit of $q_n \ll 1$. This is because the linear plasma permittivity is simply proportional to the plasma concentration. The nonlinear frequency shift coefficient due to the electron relativistic motion is $R = a_0 \omega_e^2 \omega_a q_n / V_3 4 \omega_b^2$. For homogeneous plasma ($q_n = 1$), this formula reduces to the given in Refs. 19, 24, and 41–43. The seed group velocity dispersion coefficient is $\kappa = a_0 V_3 \omega_e^2 q_n / [2 \omega_b (\omega_b^2 - \omega_e^2 q_n)]$. For homogeneous plasma ($q_n = 1$), this formula reduces to the given in Refs. 19 and 24.

The inverse bremsstrahlung rates⁴⁴ of the pump and seed pulses due to the electron-ion collision are $\nu_a = \nu_{ei} q_n \omega_e^2 / 2 \omega_a^2$ and $\nu_b = \nu_{ei} q_n \omega_e^2 / 2 \omega_b^2$. The electron-ion collision rate in inhomogeneous plasma is modeled^{19,45,46} by

$$\nu_{ei} = \frac{1}{a_0 V_3} \frac{2}{3} \sqrt{\frac{2 \pi}{m_e}} \frac{Z \Lambda n_h q_n e^4}{T_e^{1/2} (T_e + T_a + T_b + T_f)}, \quad (3)$$

where $T_a = m_e c^2 a_0^2 |a|^2$, $T_b = m_e c^2 a_0^2 |b|^2 \omega_a / \omega_b$, and $T_f = m_e c^2 a_0^2 |f|^2 \omega_a / (\omega_f \sqrt{q_n})$. Also, Λ is the Coulomb logarithm and Z is the ion state charge.

The Langmuir wave pulse damping rate, $\nu_f = \nu_{ei} / 2 + \nu_{Lnd}$, consists of both the electron-ion collision and the Landau damping rates. The linear Landau damping rate is modeled by

$$\nu_{Lnd} = \frac{1}{a_0 V_3} \frac{\sqrt{\pi} \omega_e}{(2 q_T)^{3/2}} q_n^4 \exp \left[-\frac{q_n}{2 q_T} - \frac{3}{2} \right]. \quad (4)$$

Note that for homogeneous plasma, $q_n = 1$, the model described here reduces to the same model as in Ref. 19. In the regime of homogeneous ($q_n = 1$) and collisionless plasma ($\nu_{ei} = 0$) with the assumptions that the Landau damping (ν_{Lnd}), dispersion (κ) and cubic nonlinearity (R) terms can be neglected, the solution of Eq. (1) is well known.^{47–53}

To show that Eqs. (1) and (2) conserve energy, multiply each envelope equation by its complex conjugate and its carrier frequency. Then, summing the three equations, using the resonance condition $\omega_a = \omega_b + \omega_f$, integrating in z , and using the boundary conditions of $h(z = \pm \infty, t) = 0$, gives the conservation equation

$$\frac{\partial}{\partial t} (\bar{W}_a + \bar{W}_b + \bar{W}_f) = -2(\nu_a \bar{W}_a + \nu_b \bar{W}_b + \nu_f \bar{W}_f), \quad (5)$$

where $\bar{W}_h = m_e c^2 a_0^2 \omega_a \omega_h \int_{-\infty}^{\infty} |h|^2 dz$ and $h \in \{a, b, f\}$. Similarly, multiplying Eq. (2) by $\omega_e^2 q_n$ and integrating in z gives

$$\frac{\partial}{\partial t} (\bar{W}_e) = 2(\nu_a \bar{W}_a + \nu_b \bar{W}_b + \nu_f \bar{W}_f), \quad (6)$$

where $\bar{W}_e = 1.5 \omega_e^2 \int_{-\infty}^{\infty} q_n T_e dz$, so that

$$\frac{\partial}{\partial t} (\bar{W}_a + \bar{W}_b + \bar{W}_f + \bar{W}_e) = 0. \quad (7)$$

III. NUMERICAL SIMULATIONS

To study the key features of the BRA in inhomogeneous plasma, we solve Eqs. (1) and (2) numerically. The electron density in the homogeneous section is $n_h = 10^{21} \text{ cm}^{-3}$, which corresponds to plasma wavelength $\lambda_e = 1.06 \text{ } \mu\text{m}$. We consider an electron density profile, $q_n(z) = n(z)/n_h$, given by

$$q_n(z) = \begin{cases} e^{-\frac{(z-z_p)^2}{2(0.2z_p)^2}} & 0 \leq z < z_p \\ 1 & z_p \leq z \leq (z_p + z_h) \\ e^{-\frac{(z-z_p-z_h)^2}{2(0.2z_p)^2}} & (z_p + z_h) < z \leq z_{end}, \end{cases} \quad (8)$$

where Δ_n is the plasma coupler tail length, $z_h = 20.56 \lambda_e = 21.8 \text{ } \mu\text{m}$ is the length of the homogeneous section, $z_p = \Delta_n/0.47$, and the total length of the plasma is $z_{end} = 2z_p + z_h$. The pump wavelength in vacuum is $\lambda_a = 0.351 \text{ } \mu\text{m}$, corresponding to $\omega_e/\omega_a = 0.33$. Unless mentioned otherwise, the initial pump pulse intensity is $I_{a0} = I_{br} = 84.55 \text{ PW/cm}^2$ ($a_0 = a_{br} = 0.0612$), where $a_{br} = (\omega_e/\omega_a)^{3/2} \omega_a / (2k_f c)$ is the pump amplitude and I_{br} is the pump intensity at the wavebreaking threshold.^{1,40} The 3-wave coupling constant is $V_3 = 1.14 \omega_e$. The width of the rectangular pump pulse is $\Delta_a = z_h(1/c_a + 1/c_b) \approx 0.16 \text{ ps}$, which fit to BRA in the homogeneous section. The

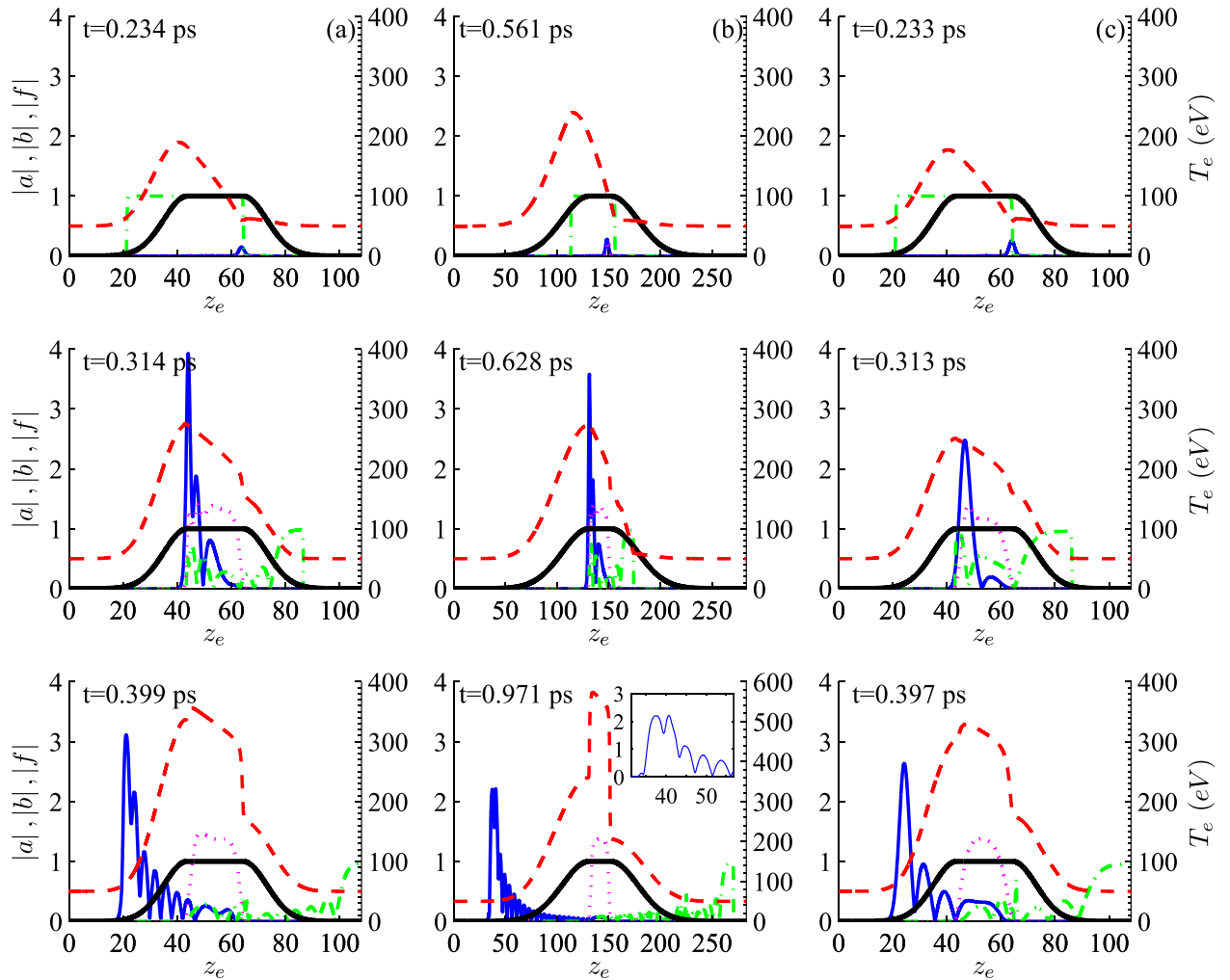


FIG. 1. The evolution of the pump, seed, and Langmuir pulses and the electron temperature for $\Delta_n/z_h = 1$ ((a) and (c)) and $\Delta_n/z_h = 3$ (b). In (a) and (b), the initial pump intensity is $I_{a0} = I_{br} = 84.55 \text{ PW/cm}^2$ and in (c), the initial pump intensity is 28.18 PW/cm^2 , which is $I_{a0} = I_{br}/3$. The initial electron temperature is $T_e(t=0, z) = 50 \text{ eV}$, $\Lambda = 3.14$, and $Z = 6$. The solid curve is the seed amplitude, the dashed-dot curve is the pump amplitude, the dotted curve is the Langmuir amplitude, and the dashed curve is the electron temperature profile. The thick curve is the plasma density profile. Here, z_e is the distance measured in electron plasma wavelength, λ_e . The inset in the bottom of (b) is the seed amplitude in the region of its maximum.

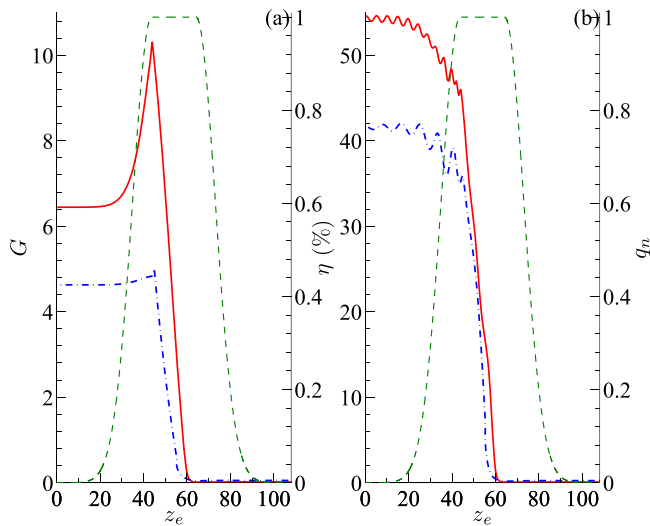


FIG. 2. (a) The local gain of the seed pulse for $I_{a0} = I_{br} = 84.55 \text{ PW/cm}^2$ (solid curve) and $I_{a0} = I_{br}/3 = 28.18 \text{ PW/cm}^2$ (dashed-dot curve). (b) The local efficiency of the seed pulse for $I_{a0} = I_{br} = 84.55 \text{ PW/cm}^2$ (solid curve) and $I_{a0} = I_{br}/3 = 28.18 \text{ PW/cm}^2$ (dashed-dot curve). In both cases, $\Delta_n/z_h = 1$. The dashed curve is the plasma density profile. Here, z_M is the location of maximum seed amplitude.

initial seed pulse has a Gaussian profile with maximum intensity of 1.5 PW/cm^2 and full width at half maximum (FWHM) of $4\pi/\omega_e = 7.04 \text{ fs}$. Here, $\Lambda = 3.14$, $Z = 6$, and $T_e(t=0, z) = 50 \text{ eV}$ ($q_T(t=0, z) = 2.02 \cdot 10^{-3}$).

Figure 1 shows the evolution of the pump, seed, and Langmuir pulses, and the electron temperature, for $\Delta_n/z_h = 1$ (Figs. 1(a) and 1(c)) and $\Delta_n/z_h = 3$ (Fig. 1(b)). In Fig. 1(c), the initial pump intensity is 28.18 PW/cm^2 , which is a third of the wavebreaking threshold. In all three cases, the BRA starts at the right edge of the homogeneous section and ends at the left edge of the homogeneous section. The seed amplitude at the plasma exit is smaller than at the edge of the

homogeneous section, while at both the plasma exit and the edge of the homogeneous section the corresponding seed fluences remain almost the same. Thus, the amplification reduction is mainly due to the non-dissipative seed dispersion effect.

For longer plasma coupler tail length with the same initial pump, the seed amplification and dispersion at the edge of the homogeneous section will be almost the same. However, the seed passes through a longer plasma coupler tail length with initial strong dispersion which, in turn, results in a longer distance over which the seed amplitude is reduced. It can be seen from Fig. 1(b) that, for $I_{a0} = I_{br}$ and $\Delta_n/z_h = 3$, the seed amplitude is reduced at the edge of the homogeneous section from about 4 to 2 at the plasma exit. In Fig. 1(b), the seed amplitude at the plasma exit is as small as the secondary spike, resulting in a non-focused pulse.

On the other hand, for smaller initial pump intensity, hence smaller Raman growth rate and for the same plasma coupler tail length, the total seed amplification at the edge of the homogeneous section will be smaller. The smaller seed amplification corresponds to a wider seed width which results in a smaller seed dispersion, so that the seed amplitude is hardly reduced in the plasma coupler tail (on the left side). In our example, for $I_{a0} = I_{br}$ and $\Delta_n/z_h = 1$ (Fig. 1(a)), the seed amplitude is reduced at the edge of the homogeneous section from about 4 to 3 at the plasma exit; while for $I_{a0} = I_{br}/3$ and $\Delta_n/z_h = 1$ (Fig. 1(c)), the seed amplitude is reduced from about 2.7 to 2.5.

Figure 2 shows the local gain (Fig. 2(a)) and efficiency (Fig. 2(b)) for the cases shown in Fig. 1(a) (Fig. 2 solid curve) and Fig. 1(c) (Fig. 2 dashed-dot curve). The local gain of the seed is defined by

$$G(t) = \frac{I_b}{I_{a0}} = \frac{c_b \omega_b}{c_a \omega_a} \max_z |b(z, t)|^2, \quad (9)$$

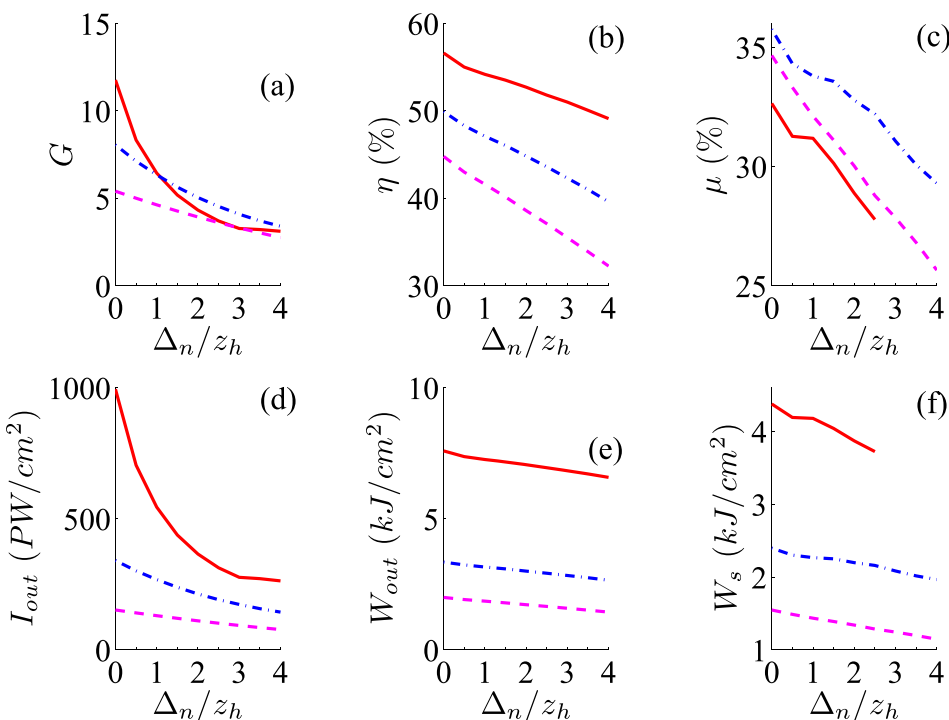


FIG. 3. The output gain (a), efficiency (b), and leading spike efficiency (c). The output intensity (d), fluence (e), and leading spike fluence (f) are also shown. The solid curve corresponds to $I_{a0} = I_{br} = 84.55 \text{ PW/cm}^2$, the dashed-dot curve corresponds to $I_{a0} = I_{br}/2 = 42.3 \text{ PW/cm}^2$, and the dashed curve corresponds to $I_{a0} = I_{br}/3 = 28.18 \text{ PW/cm}^2$.

where I_b is the maximum seed intensity and the local efficiency of the seed is defined by

$$\eta(t) = \frac{W_b}{W_{a0}} = \frac{\omega_b}{\omega_a} \frac{\int_{-\infty}^{\infty} |b(z, t)|^2 dz}{(c_a/c)(\Delta_a V_3 a_0)}, \quad (10)$$

where W_b is the seed fluence and W_{a0} is the input pump fluence. Here, the seed fluence, W_b , is calculated by integrating over space, (which is equivalent to integrating over time multiplied by the seed group velocity). To follow the evolution of the gain and efficiency in the inhomogeneous plasma, we calculate for each time the location of the maximum seed amplitude, z_M , and associate with it the calculated gain and efficiency as shown in Figure 2.

As Fig. 2(a) shows, the Raman amplification of the seed starts at the right side ($z \approx 60\lambda_e$) of the homogeneous section and ends at the left side ($z \approx 40\lambda_e$). At the left edge of the homogeneous section, the seed amplitude is the largest but with the shortest duration. Hence, at this point, the seed dispersion is the strongest. When the seed begins to pass through the plasma coupler tail (on the left side), where

resonance no longer exists, it is affected only by dispersion and by inverse bremsstrahlung. Since in both cases, the local efficiency in the plasma coupler tail (on the left side) remains approximately the same (Fig. 2(b)), the most dominant effect for the seed amplitude reduction is due to the dispersion. As the seed propagates through the plasma coupler tail (on the left side), its amplitude is decreased, and from conservation of energy, its pulse width grows. At the same time the plasma density is decreased. Hence, the dispersion effect becomes smaller as the seed transverses through the exit region. Note also that, Fig. 2 shows that for smaller initial pump intensity (dashed curve), the seed amplitude reduction should be smaller. As explained above, this is because at low amplitude the Raman compression is smaller; so for the same length of homogeneous section, the seed width at the left edge of the homogeneous section will be wider. Hence, at this point, the seed dispersion is smaller, which results in a smaller reduction in the seed amplitude as it propagates through the plasma coupler tail (on the left side).

Fig. 3 shows, in our example, the correlation of the output seed gain (a), efficiency (b), and leading spike efficiency (c) to the plasma coupler tail length and the three initial

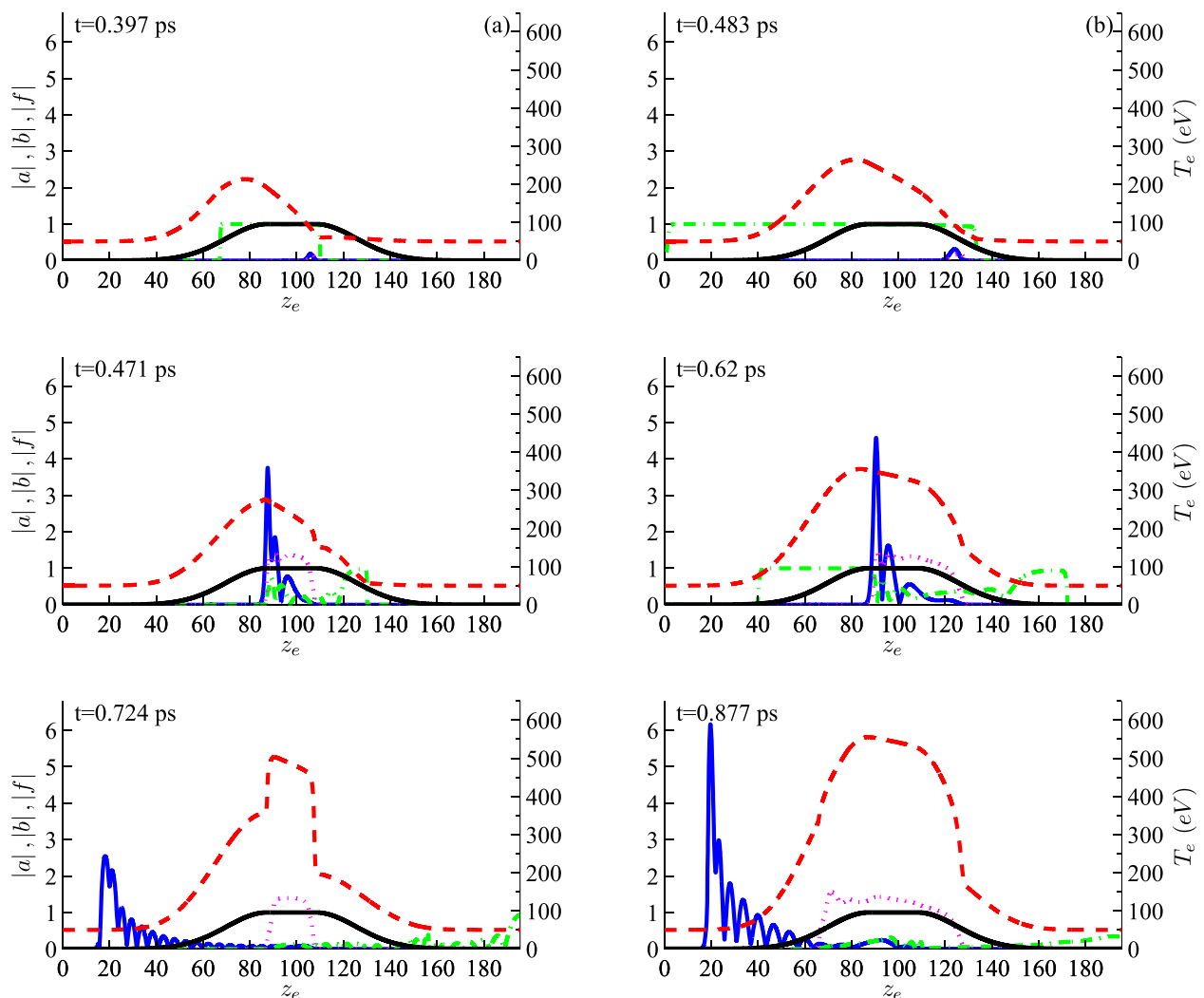


FIG. 4. The evolution of the pump, seed, and Langmuir pulses and the electron temperature for (a) non-chirped pump and seed pulses and for (b) chirped pump and seed pulses. Solid curve is the seed amplitude, dashed-dot curve is the pump amplitude, dotted curve is the Langmuir amplitude, and dashed curve is the electron temperature profile. In both cases, $\Delta_n/z_h = 2$. The solid thick curve is the plasma density profile.

pump intensity: $I_{a0} = I_{br}$ (solid curve), $I_{a0} = I_{br}/2$ (dashed-dot curve), and $I_{a0} = I_{br}/3$ (dashed curve). The output intensity (d), fluence (e), and leading spike fluence (f) are also shown. Here, the leading spike fluence is defined by $W_s = I_{out}\Delta_{out}$, where Δ_{out} is the seed width at the plasma exit. The leading spike efficiency, $\mu = W_s/W_{a0}$, is defined as the leading spike fluence to the input pump fluence ratio. Note that for $I_{a0} = I_{br}$, the leading spike fluence and efficiency are not shown because the output seed is not focused, as shown for example in Fig. 1(b).

For the three initial pump intensities shown in Fig. 3, the output gain, efficiency, and leading spike efficiency are decreased as the plasma coupler tail length is increased. As shown in Fig. 3(a), while for $I_{a0} = I_{br}$, the gain reduction is the largest, it is the smallest for $I_{a0} = I_{br}/3$ due to the dispersion effect. The largest gain reduction occurs at $\Delta_n/z_h = 1$ for $I_{a0} = I_{br}$. However, Fig. 3(b) shows that for $I_{a0} = I_{br}$ and long plasma coupler tail length, the output efficiency, η , is slightly reduced; whereas for $I_{a0} = I_{br}/3$, it is largely reduced due to the inverse bremsstrahlung.

Interestingly, Fig. 3(c) shows that the first spike efficiency is the highest for $I_{a0} = I_{br}/2$ over a large range of plasma coupler tail lengths, due to a compromise between the competitive effects of Raman growth rate, seed dispersion, and inverse bremsstrahlung. As seen in Figs. 3(d)–3(f), the output intensity, the total output fluence, and the leading spike fluence of the seed are significantly less sensitive to the plasma coupler tail length for $I_{a0} = I_{br}/2$ than for $I_{a0} = I_{br}$. But for $I_{a0} = I_{br}/2$, the leading spike intensity is about 300 PW/cm² and the fluence is 2 kJ/cm², compared to intensity of 1000 PW/cm² and fluence of 4 kJ/cm² for $I_{a0} = I_{br}$ and homogeneous plasma.

IV. DISPERSION AND INVERSE BREMSSTRAHLUNG COMPENSATION BY PUMP AND SEED CHIRPING

To compensate for the dispersion and the inverse bremsstrahlung effects, we suggest to chirp both the pump and seed pulses.

First, in order that the dispersion effect in the inhomogeneous plasma be reduced significantly, the pump pulse is chirped, so that the Raman resonance condition is satisfied throughout the whole plasma layer. In an inhomogeneous plasma, the Raman resonance condition according to Eq. (1) is

$$\omega_a - \omega_b - \omega_e = V_3 a_0 (\Delta\omega + \sigma_a - \sigma_b - \sigma_f), \quad (11)$$

where $\Delta\omega$ is the pump frequency chirp parameter that is required to satisfy Eq. (11). Since in homogeneous plasma, the Raman resonance condition is $\omega_a - \omega_b - \omega_e = 0$, the resonance condition in Eq. (11) can be simplified to the form

$$\Delta\omega = \sigma_f + \sigma_b - \sigma_a. \quad (12)$$

We can equivalently chirp the Langmuir pulse, f , with $-\Delta\omega$ chirp parameter. Hence, the equation for the Langmuir pulse becomes

$$f_t = -q_n^{1/4} a b^* + i\sigma_f f - \nu_f f - i\Delta\omega f, \quad (13)$$

which is of the same form as in Ref. 26. The right hand side of the resonance condition in Eq. (12) is a function of the location z . Hence, the pump chirping $\Delta\omega$ should be z dependent as well. Such chirping can be realized if the input pump at $z = 0$ will be chirped as a function of time, so that after sufficient time, the propagating pump will eventually have the desired spatial frequency detuning profile. In addition, the amplified seed is well localized in space-time. Theoretically, the BRA resonance condition can be satisfied through the whole plasma when chirping the pump pulse according to Eq. (12). However, the input pump intensity at the wave-breaking threshold is small in the inhomogeneous sections. Hence, to achieve high Raman amplification in most of the plasma slab, we choose initial pump intensity of $I_{a0} = 24$ PW/cm², which is at the wavebreaking threshold for electron density of $5 \cdot 10^{20}$ cm⁻³ ($q_n = 0.5$).

Second, the Gaussian seed pulse can also be chirped, a technique which might be useful even for purely homogeneous plasma.⁵⁴ Here, the chirping is initialized such that, in the absence of the pump pulse and the nonlinear relativistic effect, the seed pulse would self-contract for homogeneous density n_h and reach its shortest duration after passing a distance of $1.5z_L = 1.5(z_h + \Delta_n)$, where z_L corresponds to the section of $q_n \geq 0.5$ in the inhomogeneous plasma. The minimum seed duration at this point is $4\pi/\omega_e$, which is the same duration of the non-chirped case at the entrance to the plasma. The timing of the pump and the seed pulses were chosen such that the BRA occurs in the section of $q_n \geq 0.5$.

Figure 4 compares the evolution of the non-chirped pump, non-chirped seed, and Langmuir pulse (Fig. 4(a)) with the chirped pump, chirped seed, and Langmuir pulse (Fig. 4(b)) for the case of $\Delta_n/z_h = 2$. According to Fig. 4(a), the output intensity of the amplified non-chirped seed pulse is 365.26 PW/cm² with $3 \cdot 2\pi/\omega_e = 10.56$ fs duration and the leading spike fluence is 3.87 kJ/cm². However, the output intensity of the amplified chirped seed pulse (Fig. 4(b)) is

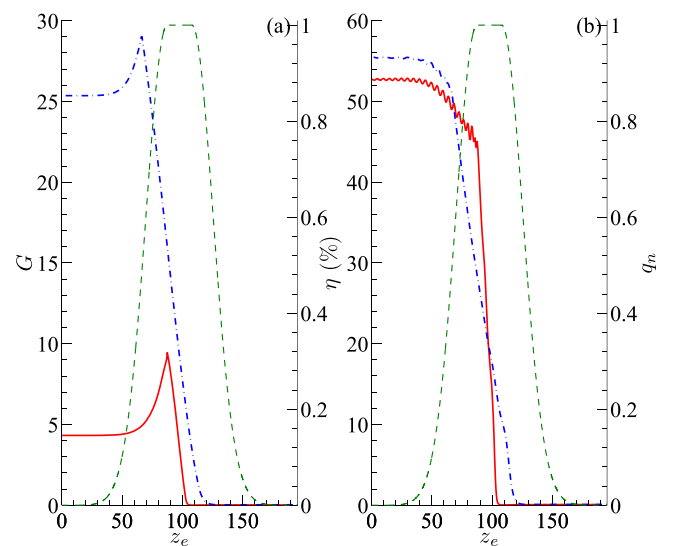


FIG. 5. (a) The local gain of the seed pulse for non-chirped pump and seed pulses (solid curve) and for chirped pump and seed pulses (dashed-dot curve). (b) The local efficiency of the seed pulse for non-chirped pump and seed pulses (solid curve) and for chirped pump and seed pulses (dashed-dot curve). In both cases, $\Delta_n/z_h = 2$.

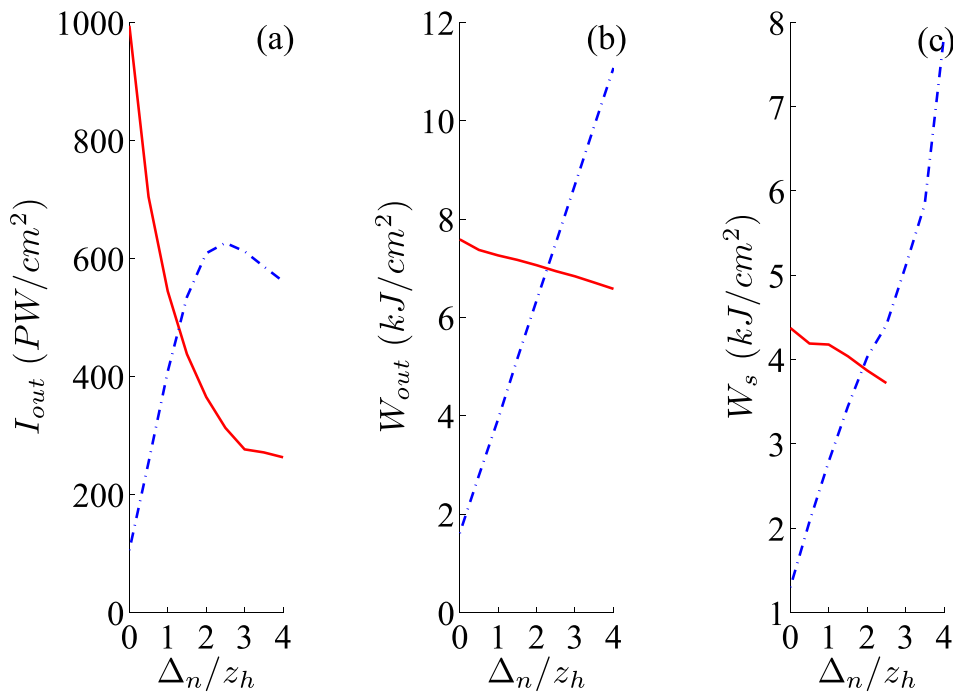


FIG. 6. The output intensity (a), fluence (b), and leading spike fluence (c). The solid curve corresponds to non-chirped pump and seed pulses and the dashed-dot curve corresponds to chirped pump and seed pulses.

608 PW/cm^2 with $1.88 \cdot 2\pi/\omega_e = 6.62$ fs duration. The leading spike fluence is $4 \text{ kJ}/\text{cm}^2$. Also, the secondary spikes of the amplified chirped seed pulse are much smaller than in the non-chirped seed pulse. These secondary spikes are also not close to the leading spike. Thus, the output pulse is significantly reshaped.

To see in more detail, the amplification and efficiency of the chirped seed pulse in this example, we show in Fig. 5(a) the local gain and in Fig. 5(b) the local fluence efficiency. Also, we compared the non-chirped seed (solid curve and it is the same as in Fig. 2) with the chirped seed and pump (dashed-dot curve). As can be seen from Figs. 5(a) and 5(b), the Raman amplification occurs over longer distance for the chirped seed and pump ($q_n \leq 0.5$) than the non-chirped seed and pump ($q_n = 1$). Since for the chirped seed and pump, the initial pump intensity ($I_{a0} = 24 \text{ PW}/\text{cm}^2$) is smaller than for the non-chirped pump and seed ($I_{a0} = 84.55 \text{ PW}/\text{cm}^2$), the chirped seed and pump has a smaller Raman growth rate. Thus, a longer plasma coupler tail length is required. Since for a given plasma coupler tail length, the resonant region length is longer in the chirped pump and seed case than in the non-chirped pump and seed case, the non-resonant region length in the chirped pump and seed case is shorter. Thus, it will be only over a somewhat shorter length that the amplified seed pulse will be subject to deleterious effects such as the inverse bremsstrahlung, while not undergoing resonant amplification. In this example, the output intensity of the chirped seed and pump is $608 \text{ PW}/\text{cm}^2$, which is higher by 65% than the intensity of the non-chirped seed pulse, which is $365.26 \text{ PW}/\text{cm}^2$. The total efficiency is similar, about 55%, with a bit higher efficiency for the chirped seed pulse. The output fluence of the first spike of the seed is about $4 \text{ kJ}/\text{cm}^2$.

Since for the chirped seed and pump, the initial pump intensity ($I_{a0} = 24 \text{ PW}/\text{cm}^2$) is smaller than the non-chirped pump and seed ($I_{a0} = 84.55 \text{ PW}/\text{cm}^2$), the smaller Raman growth rate in the case of the chirped pump and seed case

requires a longer plasma coupler tail length to achieve output intensity and efficiency larger than in the case of the non-chirped seed and pump. As seen in Figs. 6(a) and 6(b), the output intensity and fluence of the chirped seed (dashed-dot curve) is larger than the non-chirped seed (solid curve) for plasma coupler tail length at least twice the length of the homogeneous section ($\Delta_n/z_h \geq 2$). Also, as shown in Fig. 6(b) that the output fluence of the non-chirped seed is reduced for long plasma coupler tail length. This is because of the inverse bremsstrahlung effect. However, for the chirped pump and seed case, the output fluence of the chirped seed is increased for longer plasma coupler tail length. This is because the amplification length is increased for longer plasma coupler tail length and hence minimizing the inverse bremsstrahlung effect. Note that for each Δ_n/z_h , the pump chirp $\Delta\omega$ is chosen so as to satisfy Eq. (12).

In both cases of chirped seed and pump and non-chirped seed and pump, we choose the initial pump intensity at the wavebreaking threshold. This guarantees that most of the energy transferred to the Langmuir wave occurs in the resonant regions. These regions are at higher density, so wavebreaking is avoided. Hence, the fluid model describes well the Raman compression effect, where it matters.

V. CONCLUSIONS

We considered Raman compression in a plasma slab, which is comprised of a homogeneous middle section and inhomogeneous end sections, such that the electron density in each end section tapers to zero. In our specific example, the pump wavelength is $0.351 \mu\text{m}$ and the electron density in the homogeneous section is 10^{21} cm^{-3} , corresponding to $\omega_e/\omega_a = 0.33$. Though it is a specific example, it indicative of the general case of undercritical dense plasma, where both seed dispersion and inverse bremsstrahlung can be limiting effects.

We showed, for initial pump intensity at the wavebreaking threshold, a significant reduction in the output seed amplification for plasma coupler tail length longer than the homogeneous section. The amplification is strongly reduced at the exit of the homogeneous section, where the seed pulse duration is the shortest and hence the seed dispersion is the strongest. Nevertheless, the output fluence is almost not affected, since the dispersion is non-dissipative. For lower initial pump intensity, hence lower Raman growth rate, the seed amplitude is smaller and its duration longer. Hence, the seed dispersion is smaller in the plasma coupler tail (on the left side), which results in a smaller reduction of the seed amplitude and fluence. However, the output amplification and fluence are smaller than in the case of initial pump intensity at the wavebreaking threshold.

Interestingly, we showed that the first spike efficiency is highest for $I_{a0} = I_{br}/2$ over a large range of plasma coupler tail lengths. The maximum occurs due to a compromise between the competitive effects of Raman growth rate, seed dispersion, and inverse bremsstrahlung. However, the leading spike intensity and fluence are significantly smaller than in the case of initial pump intensity at the wavebreaking threshold in homogeneous plasma (zero plasma coupler tail length).

To compensate for the dispersion and inverse bremsstrahlung effects, we propose to chirp both the pump and the seed pulses such that the BRA will be in resonance over a longer plasma length, which includes both the homogeneous section and part of the inhomogeneous sections. While in the case of non-chirped pump and seed, the Raman compression stops at the edge of the homogeneous section; in this approach, the Raman compression continues in the end region and stops only at the point where the plasma density is half that of the homogeneous section. Thus, the seed dispersion after the compression stage is significantly smaller than in the case of the non-chirped pump and seed. Also, the amplified seed pulse then passes through shorter non-resonant plasma region, so that it will be less affected by deleterious effects. We showed that for plasma coupler tail length longer than the homogeneous section, the output chirped seed pulse can reach higher intensity and fluence than in the case of the non-chirped pump and seed.

The case of long end-regions may be important for the next generation of intensities, which will require larger spot-sizes with thin plasma. For such thin and dense undercritical plasma, the density may taper to zero over a distance large compared to its optimum width, thus creating the conditions wherein the measures proposed here may be useful.

ACKNOWLEDGMENTS

This work was supported by the NNSA under the SSAA Program through DOE Research Grant No. DE-AC0209-CH11466, by the RFBR Grant No. 11-02-01070 and the RFBR Grant No. 12-02-00650.

¹V. M. Malkin, G. Shvets, and N. J. Fisch, *Phys. Rev. Lett.* **82**, 4448 (1999).

²D. Strickland and G. Mourou, *Opt. Commun.* **56**, 219 (1985).

- ³M. S. Hur, R. R. Lindberg, A. E. Charman, J. S. Wurtele, and H. Suk, *Phys. Rev. Lett.* **95**, 115003 (2005).
- ⁴M. S. Hur, D. N. Gupta, and H. Suk, *J. Phys. D* **40**, 5155 (2007).
- ⁵M. S. Hur and J. S. Wurtele, *Comput. Phys. Commun.* **180**, 651 (2009).
- ⁶T.-L. Wang, D. S. Clark, D. J. Strozzi, S. C. Wilks, S. F. Martins, and R. K. Kirkwood, *Phys. Plasmas* **17**, 023109 (2010).
- ⁷H. Gareth, S. Ashutosh, and K. Ioannis, *Phys. Lett. A* **374**, 4336 (2010).
- ⁸S. Son, S. Ku, and S. J. Moon, *Phys. Plasmas* **17**, 114506 (2010).
- ⁹D. Benisti, O. Morice, L. Gremillet, E. Siminos, and D. J. Strozzi, *Phys. Plasmas* **17**, 102311 (2010).
- ¹⁰J. P. Farmer, B. Ersfeld, and D. A. Jaroszynski, *Phys. Plasmas* **17**, 113301 (2010).
- ¹¹V. V. Kozlov, S. V. Manakov, and S. Wabnitz, *Opt. Lett.* **36**, 1632 (2011).
- ¹²G. Zhe-Yi, Y. Yan, C. De-Peng, Z. Hong-Bin, M. Yan-Yun, and S. Fu-Qiu, *Chin. Phys. Lett.* **29**, 015201 (2012).
- ¹³N. A. Yampolsky and N. J. Fisch, *Phys. Plasmas* **18**, 056711 (2011).
- ¹⁴G. A. Mourou, N. J. Fisch, V. M. Malkin, Z. Toroker, E. A. Khazanov, A. M. Sergeev, T. Tajima, and B. L. Garrec, *Opt. Commun.* **285**, 720 (2012).
- ¹⁵D. S. Clark and N. J. Fisch, *Phys. Plasmas* **8**, 3363 (2003).
- ¹⁶N. J. Fisch and V. M. Malkin, *Phys. Plasmas* **10**, 2056 (2003).
- ¹⁷V. M. Malkin, G. Shvets, and N. J. Fisch, *Phys. Plasmas* **12**, 044507 (2005).
- ¹⁸V. M. Malkin, G. Shvets, and N. J. Fisch, *Phys. Rev. E* **75**, 026404 (2007).
- ¹⁹A. A. Balakin, N. J. Fisch, G. M. Fraiman, V. M. Malkin, and Z. Toroker, *Phys. Plasmas* **18**, 102311 (2011).
- ²⁰A. A. Solodov, V. M. Malkin, and N. J. Fisch, *Phys. Plasmas* **10**, 2540 (2003).
- ²¹V. M. Malkin and N. J. Fisch, *Phys. Plasmas* **17**, 073109 (2010).
- ²²R. M. G. M. Trines, F. Fiuza, R. Bingham, R. A. Fonseca, L. O. Silva, R. A. Cairns, and P. A. Norreys, *Nat. Phys.* **7**, 87 (2011).
- ²³R. M. G. M. Trines, F. Fiuza, R. Bingham, R. A. Fonseca, L. O. Silva, R. A. Cairns, and P. A. Norreys, *Phys. Rev. Lett.* **107**, 105002 (2011).
- ²⁴V. M. Malkin, Z. Toroker, and N. J. Fisch, *Phys. Plasmas* **19**, 023109 (2012).
- ²⁵V. M. Malkin and N. J. Fisch, *Phys. Rev. Lett.* **99**, 205001 (2007).
- ²⁶V. M. Malkin, G. Shvets, and N. J. Fisch, *Phys. Rev. Lett.* **7**, 1208 (2000).
- ²⁷M. N. Rosenbluth, *Phys. Rev. Lett.* **29**, 565 (1972).
- ²⁸A. A. Balakin, D. V. Kartashov, A. M. Kiselev, S. A. Skobelev, A. N. Stepanov, and G. M. Fraiman, *JETP Lett.* **80**, 12 (2004).
- ²⁹X. Yang, G. Vieux, E. Brunetti, J. P. Farmer, B. Ersfeld, S. M. Wiggins, R. C. Issac, G. H. Welsh, and D. A. Jaroszynski, *Proc. SPIE* **8075**, 80750G (2011).
- ³⁰G. Vieux, A. Lyachev, X. Yang, B. Ersfeld, J. P. Farmer, E. Brunetti, R. C. Issac, G. Raj, G. H. Welsh, S. M. Wiggins, and D. A. Jaroszynski, *New J. Phys.* **13**, 063042 (2011).
- ³¹R. K. Kirkwood, E. Dewald, C. Niemann, N. Meezan, S. C. Wilks, D. W. Price, O. L. Landen, J. Wurtele, A. E. Charman, R. L. N. J. Fisch, V. M. Malkin, and E. J. Valeo, *Phys. Plasmas* **14**, 113109 (2007).
- ³²J. Ren, S. Li, A. Morozov, S. Suckewer, N. A. Yampolsky, V. M. Malkin, and N. J. Fisch, *Phys. Plasmas* **15**, 056702 (2008).
- ³³Y. Ping, I. Geltner, N. J. Fisch, G. Shvets, and S. Suckewer, *Phys. Rev. E* **62**, R4532 (2000).
- ³⁴Y. Ping, I. Geltner, A. Morozov, N. J. Fisch, and S. Suckewer, *Phys. Rev. E* **66**, 046401 (2002).
- ³⁵Y. Ping, W. Cheng, S. Suckewer, D. S. Clark, and N. J. Fisch, *Phys. Rev. Lett.* **92**, 175007 (2004).
- ³⁶W. Cheng, Y. Avitzour, Y. Ping, S. Suckewer, N. J. Fisch, M. S. Hur, and J. S. Wurtele, *Phys. Rev. Lett.* **94**, 045003 (2005).
- ³⁷C. H. Pai, M. W. Lin, L. C. Ha, S. T. Huang, Y. C. Tsou, H. H. Chu, J. Y. Lin, J. Wang, and S. Y. Chen, *Phys. Rev. Lett.* **101**, 065005 (2008).
- ³⁸K. Mima, M. M. Skoric, S. Miyamoto, A. Maluckov, and M. S. Jovanovic, *AIP Conf. Proc.* **406**, 381 (1997).
- ³⁹S. I. Braginskii, "Transport processes in a plasma," in *Review of Plasma Physics*, edited by M. A. Leontovich (Consultants Bureau, New York, 1965), Vol. 1, pp. 205–311.
- ⁴⁰W. L. Kruer, *The Physics of Laser Plasma Interactions* (Addison-Wesley, Reading, MA, 1988).
- ⁴¹A. G. Litvak, *Zh. Eksp. Teor. Fiz.* **57**, 629 (1969) [*Sov. Phys. JETP* **30**, 344 (1970)].
- ⁴²C. Max, J. Arons, and A. B. Langdon, *Phys. Rev. Lett.* **33**, 209 (1974).
- ⁴³G.-Z. Sun, E. Ott, Y. C. Lee, and P. Guzdar, *Phys. Fluids* **30**, 526 (1987).
- ⁴⁴I. P. Shkarofsky, T. W. Johnston, and M. P. Bachynsky, *The Particle Kinetics of Plasmas* (Addison-Wesley, Reading, MA, 1966).
- ⁴⁵A. Balakin, G. Fraiman, and V. Mironov, *Phys. Plasmas* **8**, 2502 (2001).

- ⁴⁶A. Brantov, W. Rozmus, and R. Sydora, *Phys. Plasmas* **10**, 3385 (2003).
- ⁴⁷G. L. Lamb, Jr., *Phys. Lett. A* **29**, 507 (1969).
- ⁴⁸G. L. Lamb, Jr., *Rev. Mod. Phys.* **43**, 99124 (1971).
- ⁴⁹G. L. Lamb, Jr., *Elements of Soliton Theory* (Wiley, New York, 1980).
- ⁵⁰V. E. Zakharov, *JETP Lett.* **32**, 589 (1980).
- ⁵¹S. V. Manakov, *JETP Lett.* **35**, 237 (1982).
- ⁵²V. A. Gorbunov, V. B. Ivanov, S. B. Papernyi, and V. R. Startsev, *Izv. Akad. Nauk SSSR, Ser. Fiz.* **48**, 1580 (1984) [*Bull. Acad. Sci. USSR, Phys. Ser. (Engl. Transl.)* **48**, 120 (1984)].
- ⁵³J. Coste and C. Montes, *Phys. Rev. A* **34**, 3940 (1986).
- ⁵⁴Z. Toroker, V. M. Malkin, and N. J. Fisch, *Phys. Rev. Lett.* **109**, 085003 (2012).